Chemical Engineering Journal 149 (2009) 232–241

Contents lists available at ScienceDirect

Chemical Engineering Journal

journal homepage: www.elsevier.com/locate/cej

Analysis of membrane pore blocking models adapted to crossflow ultrafiltration in the ultrafiltration of PEG

M. Cinta Vincent Vela [a], Silvia Álvarez Blanco [a,*], Jaime Lora García [a], Enrique Bergantiños Rodríguez [b]

[a] Department of Chemical and Nuclear Engineering, Polytechnic University of Valencia, C/Camino de Vera s/n, 46022 Valencia, Spain
[b] Department of Chemical Engineering, Polytechnical Institute José A. Echeverría, Ave. 114, No. 11901, Havana, Cuba

ARTICLE INFO

Article history:
Received 10 July 2008
Received in revised form 13 October 2008
Accepted 30 October 2008

Keywords:
Ultrafiltration
Crossflow
Fouling
Blocking model
Gel layer model

ABSTRACT

In this work Hermia's models adapted to crossflow ultrafiltration were used to investigate the fouling mechanisms involved in the ultrafiltration of polyethylene glycol (PEG). Although PEG has been very often used as a standard macromolecule in ultrafiltration experiments to test flux decline models, it has not been used to test Hermia's models adapted to crossflow ultrafiltration. This work analyses the different fouling mechanisms that may occur at different stages of the ultrafiltration process. Fitted Hermia's models parameters are also analyzed for the experimental conditions tested on the basis of their physical meaning.

Ultrafiltration experiments were performed with ceramic membranes supplied at different experimental conditions: feed flow rates and transmembrane pressures (TMPs). The results showed that the phenomenon controlling fouling was intermediate blocking for the highest TMP and the lowest crossflow velocity tested. For lower TMPs and/or higher a crossflow velocities, complete blocking or intermediate blocking controlled the fouling process. The analysis of the fouling mechanisms performed dividing the filtration curves in different regions revealed that complete blocking was dominant for a TMP of 0.3 MPa and a crossflow velocity of 1 m/s and in the case of a TMP of 0.4 MPa and a crossflow velocity of 2 m/s.

1. Introduction

Industrial ultrafiltration was initially developed for the treatment of wastewaters and sewage [1] to remove particulate and macromolecular materials [2]. Its applicability has now widened considerably to include other fields such us water treatment, chemicals processing, food processing and biotechnology [3]. Some widely spread examples of environmental applications of ultrafiltration for wastewater treatment are: paint removal from electrocoating painting tanks [4]; cheese whey concentration to separate, fractionate and recover proteins before the final disposal [3]; wash water treatment from printing processes [4]; laundry wastewater treatment [2]; recovery of nonbiodegradable sizing agents from wash water in the textile industry [5]; oily wastewater treatment [6] from the metalworking [7], the food processing [3], the textile [5], the printing [4], the leather and tanning [8] and the pulp and paper [4,9] industries; etc. In many of these applications ultrafiltration is used to separate macromolecular pollutants from wastewaters.

Membrane fouling in crossflow membrane ultrafiltration is a key factor affecting the economic and technological viability of ultrafiltration processes, which essentially depend on the permeate fluxes obtained and their stability with time [2]. The typical variation of permeate flux with time is an initial rapid decrease followed by a long and gradual flux decline [10].

Consequently, modelling permeate flux decline (i.e. fouling) in the ultrafiltration of macromolecules is important from the economic and technological point view.

Membrane structure has an important influence in improving permeate flux [11]. If the membrane pores are larger than the size of the solute molecules, these molecules can enter the membrane pores causing irreversible fouling. When the opposite occurs, the membrane pores are smaller than the size of the solute molecules present in the feed solution, these molecules accumulate over the membrane surface causing pore sealing and/or the formation of a gel layer. Finally, solute molecules of a similar size to that of the membrane pores may result in a partial blocking of them.

There are many studies focused on empirical models for the description of permeate flux decline with time [12,13]. Although empirical models are very precise, they cannot adequately explain the fouling mechanisms involved in membrane filtration. Theoretical models can partially contribute to the understanding of the fouling phenomena. However, the models found in the literature that are completely theoretical have failed to accurately predict permeate flux decline with time without using experimental data to estimate at least one of their model parameters. Therefore,

* Corresponding author. Tel.: +34 963877000x76383 fax: +34 963877639.
E-mail address: sialvare@iqn.upv.es (S. Álvarez Blanco).

1385-8947/$ – see front matter © 2008 Elsevier B.V. All rights reserved.
doi:10.1016/j.cej.2008.10.027

Nomenclature

a	specific resistance of the gel layer (m kg^{-1})
a_p	radius of the solute molecule (m)
A	membrane area (m^2)
A_0	membrane porous surface (m^2)
CFV	crossflow velocity (m/s)
J_0	initial permeate flux (m/s)
J_P	permeate flux (m/s)
J_{Pss}	steady-state permeate flux (m/s)
K	constant in Eq. (1) (units depend on the parameter n in Eq. (1))
K_B	parameter in Eq. (7) in the standard blocking model that represents the decrease in the cross-sectional area of membrane pores per unit of the total volume permeated through the membrane (m^{-1})
K_C	constant in Eq. (3) that corresponds to the complete blocking model for crossflow filtration (m^{-1})
K_{CF}	phenomenological coefficient—constant in Eq. (2) that depends on the fouling mechanism (units depend on the parameter n in Eq. (2))
K_{gl}	constant in Eq. (8) that corresponds to the gel layer formation model for crossflow filtration (s/m^2)
K_G	constant in Eq. (9) in the gel layer formation model for crossflow filtration that represents the gel layer mass per unit of the total volume permeated through the membrane (kg m^{-3})
K_i	constant in Eq. (5) that corresponds to the intermediate blocking model for crossflow filtration (m^{-1})
K_s	constant in Eq. (6) that corresponds to the standard blocking model (m$^{-1/2}$ s$^{-1/2}$)
n	constant in Eq. (1) that depends on the fouling mechanism (dimensionless)
R_m	membrane resistance (m^{-1})
t	time (s)
V	accumulated permeate volume (m^3)
X_m	solute mass fraction over the membrane surface (dimensionless)

Greek letters

ρ_m	density of the feed solution over the membrane surface (kg/m^3)
ρ_s	solute density (kg/m^3)
Ψ	solute form factor (dimensionless)

semi-empirical models whose parameters have a physical meaning represent a suitable solution to achieve an accurate prediction of permeate flux decline in ultrafiltration and explain the fouling mechanisms at the same time.

In this work the effects of transmembrane pressure (TMP) and crossflow velocity in the crossflow ultrafiltration of polyethylene glycol (PEG) were investigated. The empirical models to describe permeate flux decline presented by Hermia [14] and recently modified for crossflow filtration by Field et al. [10] were used to identify the fouling mechanism involved during the ultrafiltration process. These models, whose parameters have a physical meaning, are based on classical constant pressure dead-end filtration equations. This work analyzes Hermia's models adapted to crossflow filtration with linear solute molecules of PEG. PEG has been very often used as a standard macromolecule in ultrafiltration experiments to test proposed flux decline models [15,16]. However, it has not been used to test Hermia's models adapted to crossflow filtration. This work analyzes the fitted results of Hermia's models adapted to crossflow filtration and compares them to the experimental data obtained at different experimental conditions. The experimental conditions were selected to cover all the possible fouling mechanisms that can occur with the selected solute molecule and the selected membrane. This work also analyses the filtration curves by dividing them in different regions that correspond to different fouling mechanisms. Thus, the different fouling mechanisms that may occur at different stages of the ultrafiltration process may be found.

2. Modelling

Hermia [14] developed four empirical models for dead-end filtration based on constant pressure filtration laws that correspond to four basic types of fouling: complete blocking, intermediate blocking, standard blocking and cake layer formation. The type of fouling considered depends on the value of the parameter n in Eq. (1).

$$\frac{d^2t}{dV^2} = K\left(\frac{dt}{dV}\right)^n \tag{1}$$

These models were modified to account for fouling removal mechanisms from the membrane surface [10], resulting in the following general differential equation (Eq. (2)).

$$-\frac{dJ_P}{dt} = K_{CF}(J_P - J_{Pss})J_P^{2-n} \tag{2}$$

This equation is the general equation for Hermia's models adapted to crossflow ultrafiltration, which will be named as "models" in this work. Typical values for the parameter n depending on the type of fouling are the following: complete blocking ($n=2$), intermediate blocking ($n=1$), standard blocking ($n=3/2$) and gel layer formation ($n=0$). The constant K_{CF} depends on the TMP, the dynamic viscosity of the permeate, the blocked area per unit of permeate flux and the membrane resistance, R_m. The membrane resistance is the intrinsic membrane resistance determined using pure water as feed.

The parameters considered by these models have a physical meaning and contribute to the comprehension of the mechanisms involved in membrane fouling.

2.1. Complete blocking model for crossflow filtration ($n=2$)

According to this model, it is assumed that each solute molecule arriving at the membrane surface participates in blocking by means of pore sealing. Moreover, a molecule never settles over another molecule that has been previously deposited on the membrane surface. The permeate flux through the unblocked pores is unaffected, thus the fractional reduction in permeate flux is equal to the fractional reduction in the membrane surface area corresponding to unblocked pores. This type of fouling occurs when the size of the solute molecules is greater than the size of the membrane pores. Therefore, pore blocking takes place over the membrane surface and not inside the membrane pores [17].

To adapt the complete blocking Hermia model to crossflow filtration a term representing a removal rate of molecules from the pore entrances is added and Eq. (3) is deduced.

$$J_P = J_{Pss} + (J_0 - J_{Pss})\,e^{-K_C J_0 t} \tag{3}$$

The parameter K_c represents the membrane surface blocked per unit of total volume permeated through the membrane and unit of initial membrane surface porosity. This parameter can be expressed as follows [18]:

$$K_c = \frac{3}{4}\frac{\rho_m X_m}{\rho_s a_p \Psi} \tag{4}$$

where ρ_m is the density of the feed solution over the membrane surface, ρ_s is the solute density, X_m is the solute mass fraction over the membrane surface, a_p is the radius of the solute molecule and Ψ is the solute form factor which is related to the ratio of the major to the miner dimension of the molecule. The parameters ρ_m and X_m depend on the solute concentration over the membrane surface, the solute density and the solvent density.

2.2. Intermediate blocking model for crossflow filtration (n = 1)

This model considers that one membrane pore is not necessarily blocked by one solute molecule; the probability of landing upon molecules already on the surface is taken into account [10]. Therefore, the intermediate blocking model is less restrictive because it considers that some molecules may settle over others. The non-blocked membrane surface diminishes with time [19], thus the probability of a molecule blocking a membrane pore reduces continuously with time. Intermediate blocking occurs when the solute molecule size is similar to the membrane pore size, thus some molecules can obstruct a membrane pore entrance without blocking the pore completely. The physical model leads to Eq. (5).

$$J_P = \frac{J_0 J_{Pss}\, e^{K_i J_{Pss} t}}{J_{Pss} + J_0(e^{K_i J_{Pss} t} - 1)} \tag{5}$$

The parameter K_i is equal to the parameter K_c in Eq. (4) [19]. The parameter K_i represents as well the membrane surface blocked per unit of total volume permeated through the membrane and unit of initial membrane surface porosity.

2.3. Standard blocking model for crossflow filtration (n = 3/2)

This model considers that molecules enter the membrane pores and deposit over the pore walls due to the irregularity of pore passages, reducing the membrane pore volume. Some molecules are not simply deposited over the internal surface of the membrane pores since they are adsorbed over the pore walls. This type of fouling is caused by molecules smaller than the membrane pore size and pore blocking occurs inside the membrane pores [20]. As a result, the volume of membrane pores decreases proportionally to the filtered permeate volume. The decrease in the volume of membrane pores with time is equal to the decrease in their cross section. It is considered that membrane pores have a constant length and diameter along the whole membrane. Besides, as fouling is caused by internal pore blocking, fouling becomes independent of the crossflow velocity and no limiting value for the permeate flux is attained, i.e. steady-state permeate flux is zero for long time scales [21]. The back transport diffusion of solute molecules from the membrane surface to the bulk feed solution does not occur [10]. Therefore, the equation that describes this model coincides with the one used for dead-end filtration (Eq. (6)) [18].

$$J_P = \frac{J_0}{(J_0 + J_0^{1/2} K_s t)^2} \tag{6}$$

The parameter K_s is defined in Eq. (7) and represents the volume of solid retained per unit of filtrate volume, membrane thickness and inverse membrane surface porosity.

$$K_s = 2\frac{K_B}{A_0} A J_0^{1/2} \tag{7}$$

In Eq. (7) K_B represents the decrease in the cross-sectional area of membrane pores (due to adsorption on the pore walls) per unit of total volume permeated through the membrane, A_0 is the membrane porous surface and A is the membrane area.

2.4. Gel layer formation model for crossflow filtration (n = 0)

In this case, solute molecules do not enter the membrane pores, they form a gel layer over the membrane surface [11]. Therefore, pore blocking is neglected although for both the pore blocking model and the gel layer formation model [17] solute molecules are greater than the membrane pores and do not enter them. The resulting equation is Eq. (8) [11].

$$t = \frac{1}{K_{gl} J_{Pss}^2} \ln\left[\left(\frac{J_P}{J_0}\frac{J_0 - J_{Pss}}{J_P - J_{Pss}}\right) - J_{Pss}\left(\frac{1}{J_P} - \frac{1}{J_0}\right)\right] \tag{8}$$

The parameter K_{gl} is given by Eq. (9) [10]. This parameter represents a ratio between the characteristics of the gel layer and those of the unfouled membrane.

$$K_{gl} = \frac{aK_G}{J_0 R_m} \tag{9}$$

In Eq. (9) a is the specific resistance of the gel layer, K_G represents the gel layer mass per unit of total volume permeated through the membrane and R_m is the intrinsic membrane resistance determined using pure water as feed. The parameter K_G is related to the filtrate density, the mass fraction of solutes in slurry, the mass ratio of wet to dry gel and the membrane area. The specific resistance of the gel layer, a, represents the ratio of gel layer resistance and the accumulated solute mass per unit area of the membrane surface and it depends on solute density, solute radius and gel layer porosity.

It must be noticed that all the models above mentioned account for the effect of temperature since they are all dependent on initial permeate flux, J_0, which depends on permeate viscosity and is highly influenced by the operating temperature. Moreover, model constants are dependent on the density of the feed solution that is also influenced by temperature. Solute adsorption on the membrane surface also is influenced by temperature [22]. The nature of this adsorption can be exothermic [23] (adsorption decreases with an increase in temperature) or endothermic [24] (adsorption increases with an increase in temperature). Adsorption of foulants onto the membrane surface occurs by diffusion of foulants to membrane surface followed by their interaction. Therefore, it is slightly influenced by tangential shear [25]. The effect of adsorption may be higher in the case of the standard blocking model [26] since, adsorption may occur inside the pores, which represent a higher area than that of the membrane surface.

3. Experimental

Carbosep M2 monotubular ceramic membranes supplied by Orelis, S.A. (France) with a molecular weight cut-off (MWCO) of 15 kDa were used in the experiments. The membrane area was 35.5 cm^2 with an internal diameter of 6 mm.

Polyethylene glycol (PEG) of 35,000 g/mol molecular weight was selected as the feed solute because it has been very often used as a standard macromolecule in fouling ultrafiltration tests carried out for modelling purposes [15,16]. The PEG used in the preparation of the feed solution was supplied by Merck-Schuchardt (Germany). The feed solution for the experiments was prepared by dissolving the PEG in deionised water until a concentration of 5 g/L was achieved.

The experiments were performed at different feed flow rates (1, 2 and 3 m/s), transmembrane pressures (TMPs) (0.1, 0.2, 0.3 and 0.4 MPa) and at a constant feed concentration (5 g/L). All the experiments were carried out at a constant temperature (25 °C). Ultrafiltration tests were performed with the ultrafiltration pilot plant described elsewhere [27,28]. Both the permeate and the retentate were recycled back to the feed tank. Therefore the concentration in the feed tank remained constant. Eventually, samples

of feed and permeate were taken to measure their Chemical Oxygen Demand (COD) and to calculate the membrane retention of PEG. COD Cell Test supplied by Merck (Germany) was used. The pilot plant was stopped after 7 h of operation, time enough to reach quasi steady-state conditions.

Initial membrane pure water permeability was determined in a standard initial non-fouling experiment consisting of several tests performed with deionised water under different TMPs (0.1, 0.2, 0.3 and 0.4 MPa). In these tests the crossflow velocity was set to 3 m/s, while the temperature was set to 25 °C as this was the temperature used in the fouling experiments.

The membrane was cleaned at 40 °C with an aqueous NaOH solution of 0.2% (w/w) in deionised water. The NaOH was supplied by Panreac (Spain). Once the cleaning process was finished, the water permeability of the membrane was measured with deionised water at a temperature of 25 °C, a TMP of 0.3 MPa and a crossflow velocity of 3 m/s. The cleaning protocol managed to recover initial membrane pure water permeability. Consequently, the same membrane was used in all the experiments.

4. Results and discussion

In the standard initial non-fouling experiment a linear relationship between pure water permeate flux and TMP was observed. This linear relationship was: J_P (L/h m^2) = 575.22TMP (MPa) with a measure of fit of R^2 = 0.9979.

Despite the great differences between the molecular weight of PEG, 35,000 g/mol, and the MWCO of the membrane, 15,000 g/mol, measured membrane PEG retention revealed that some PEG molecules passed through the membrane for high TMPs and low crossflow velocities. Several facts can explain this: the molecular weight distribution of the PEG used in the experiments and the elongated and non-spherical shape of PEG molecules.

Figs. 1–12 show the fitting of the experimental results to Hermia's models. The fitting procedure is performed with the Levenberg–Marquardt algorithm with MathCad®. The measures of fit, as per the R^2s, are shown in Table 1. When the values of R^2 obtained with the same model are compared for different operating conditions (see Table 1 and Figs. 1–12), it can be deduced that not always higher values of R^2 correspond to a better fit of the model. This has been previously reported by Gu [29]. Gu demonstrated the across-sample incomparability of R^2. As an example, Table 1 shows that the value of R^2 is greater for a crossflow velocity of 1 m/s and a TMP of 0.4 MPa than in the case of a crossflow velocity of 1 m/s and a TMP of 0.1 MPa for the complete blocking model. However, Fig. 1 shows that the best predictions were obtained for a TMP of 0.1 MPa. This performance was also observed for all the models considered in this work for most of the experimental conditions tested (see Figs. 1–12 and Table 1). Therefore, it can be concluded that it is adequate to compare the values of the R^2 for the different models and the same experimental conditions and it is inadequate to compare the values of R^2 for the different experimental conditions and the same model.

Figs. 1–3 show the fitting of the experimental results to the complete blocking model. The figures reveal that accurate model fittings are obtained for all the experimental conditions tested. Nevertheless, differences between experimental data and fitted results are the highest for a TMP of 0.4 MPa and a crossflow velocity of 1 m/s (Fig. 1). According to the complete blocking model assumptions

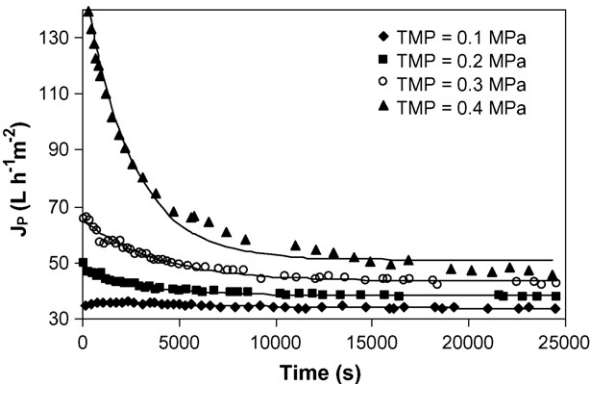

Fig. 1. Complete blocking model for crossflow filtration predictions for a crossflow velocity of 1 m/s and a solute concentration of 5 g/L for the Carbosep M2 membrane.

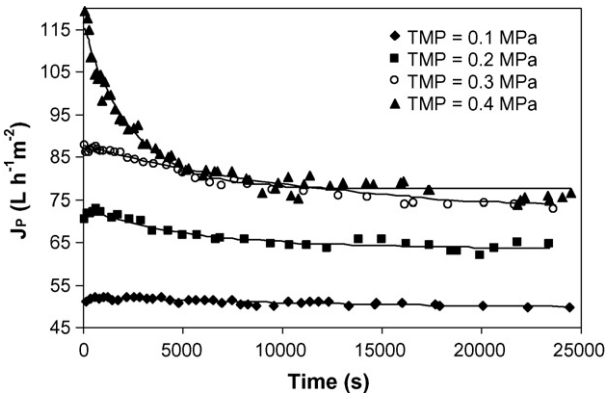

Fig. 2. Complete blocking model for crossflow filtration predictions for a crossflow velocity of 2 m/s and a solute concentration of 5 g/L for the Carbosep M2 membrane.

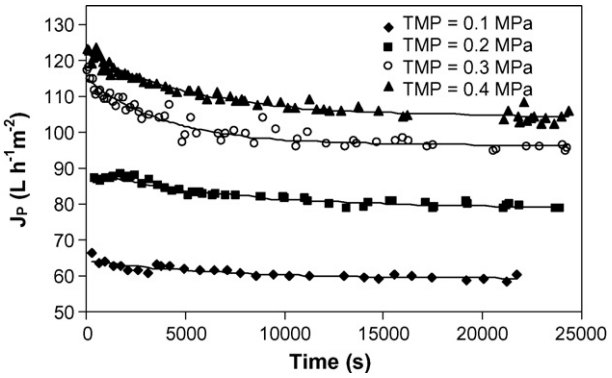

Fig. 3. Complete blocking model for crossflow filtration predictions for a crossflow velocity of 3 m/s and a solute concentration of 5 g/L for the Carbosep M2 membrane.

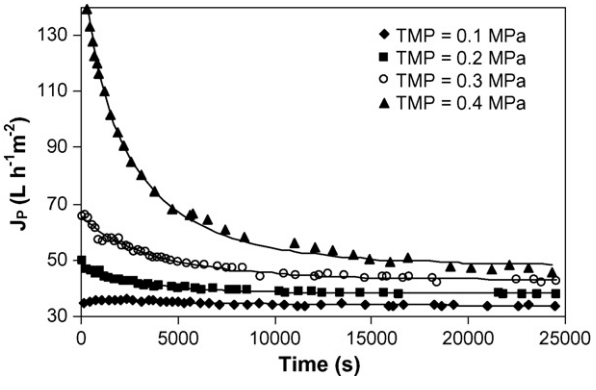

Fig. 4. Intermediate blocking model for crossflow filtration predictions for a crossflow velocity of 1 m/s and a solute concentration of 5 g/L for the Carbosep M2 membrane.

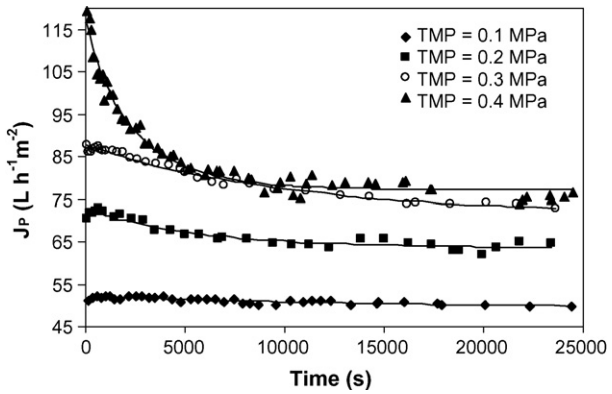

Fig. 5. Intermediate blocking model for crossflow filtration predictions for a crossflow velocity of 2 m/s and a solute concentration of 5 g/L for the Carbosep M2 membrane.

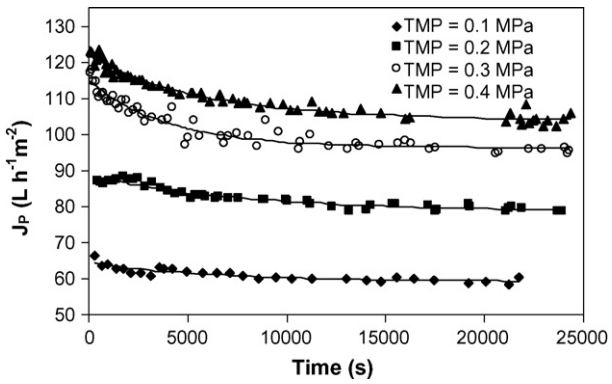

Fig. 6. Intermediate blocking model for crossflow filtration predictions for a crossflow velocity of 3 m/s and a solute concentration of 5 g/L for the Carbosep M2 membrane.

mentioned in Section 2, differences between experimental data and fitted results can be related to the fact that some PEG molecules permeated through the membrane for those experimental conditions. This is due to the fact that the highest probability of solute molecules arriving to the permeate side occurs for low crossflow velocities and high TMPs as it was experimentally demonstrated (measured PEG retention of 86.1 ± 2%). For these experimental conditions, the accumulation of solute near the membrane surface is the highest. High driving forces, TMPs, enhance convection forces towards the membrane surface, whilst low crossflow velocities decrease the surface renewal phenomenon.

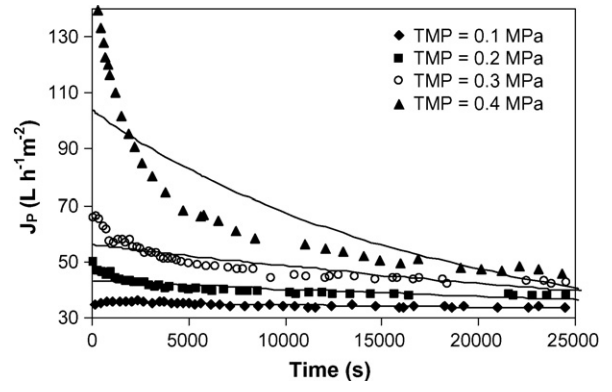

Fig. 7. Standard blocking model for crossflow filtration predictions for a crossflow velocity of 1 m/s and a solute concentration of 5 g/L for the Carbosep M2 membrane.

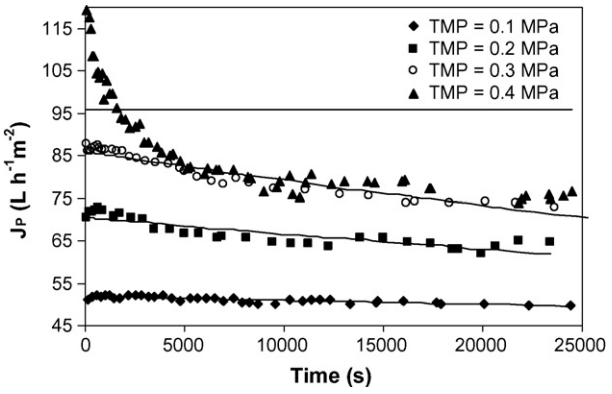

Fig. 8. Standard blocking model for crossflow filtration predictions for a crossflow velocity of 2 m/s and a solute concentration of 5 g/L for the Carbosep M2 membrane.

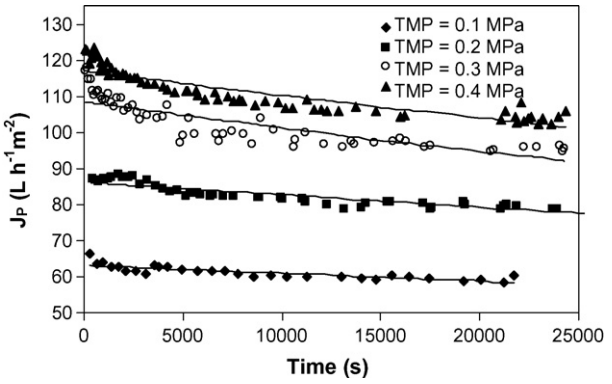

Fig. 9. Standard blocking model for crossflow filtration predictions for a crossflow velocity of 3 m/s and a solute concentration of 5 g/L for the Carbosep M2 membrane.

Figs. 4–6 show the fitting of the experimental permeate flux to the intermediate blocking model for all the experimental conditions tested. The hypothesis of the intermediate blocking model can be expected to take place for the experimental conditions tested in this work since solute molecules are not being completely retained by the membrane. Moreover, as the intermediate blocking model describes more accurately a real ultrafiltration process than the complete blocking model, better predictions are expected for the intermediate blocking model for the experimental conditions tested in this work. As a matter of fact, the intermediate blocking model fits accurately the experimental data for all the operating conditions considered in this work, even for those experimental conditions in which the complete blocking model fitted the worst,

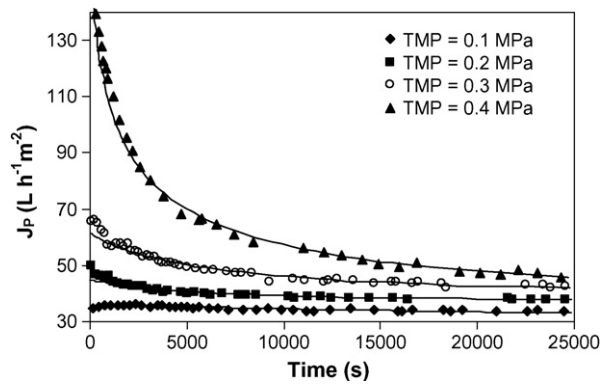

Fig. 10. Gel layer formation model for crossflow filtration predictions for a crossflow velocity of 1 m/s and a solute concentration of 5 g/L for the Carbosep M2 membrane.

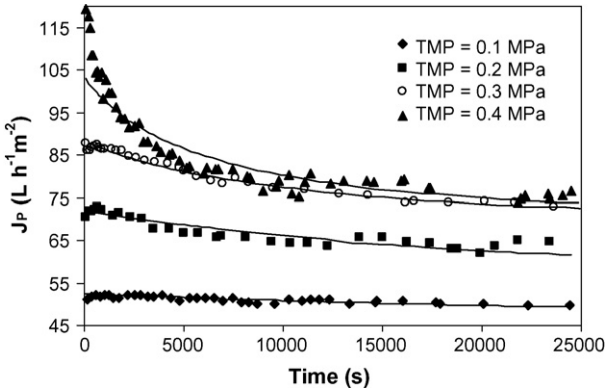

Fig. 11. Gel layer formation model for crossflow filtration predictions for a crossflow velocity of 2 m/s and a solute concentration of 5 g/L for the Carbosep M2 membrane.

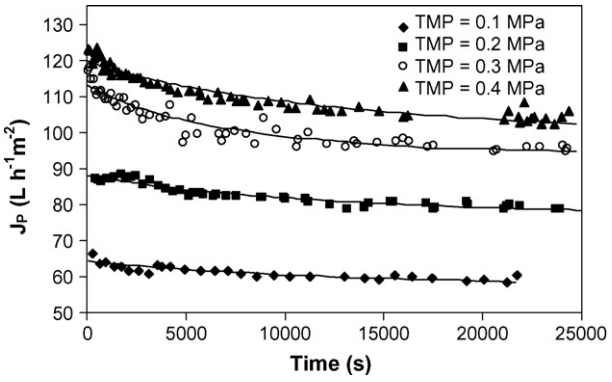

Fig. 12. Gel layer formation model for crossflow filtration predictions for a crossflow velocity of 3 m/s and a solute concentration of 5 g/L for the Carbosep M2 membrane.

these are a crossflow velocity of 1 m/s and a TMP of 0.4 MPa. For these experimental conditions the value of the R^2 for the complete blocking model is 0.988 whereas for the intermediate blocking model the reported value is 0.997 (Table 1).

Figs. 7–9 show that the fitting of the standard blocking model to the experimental results is not very good, particularly for the experimental conditions that correspond to a high variation of permeate flux with time, these are low crossflow velocities and high TMPs. Accurate predictions of permeate flux decline with time were obtained when variations in permeate flux decline with time are moderate. The reason for this can be found in the fact that measured membrane PEG retention was high for the experimental conditions tested because PEG molecules were higher than the membrane pores. In addition, the standard blocking model does not account for the effect of crossflow velocity on permeate flux. As a result, the worst permeate flux predictions obtained in this work were for the standard blocking model (see Table 1).

Figs. 10–12 illustrate the fitting of the gel layer formation model to the experimental data obtained in this work. As it was for the models already analyzed in this work, in this case model predictions are accurate when permeate flux decline with time is moderate. It must be pointed out that in the experiments performed in this work most of the PEG molecules are retained by the membrane. When permeate flux decline with time is noticeable, accurate model predictions are obtained for the experimental conditions tested for which a gel layer is more likely to form, these are a crossflow velocity of 1 m/s and a TMP of 0.4 MPa. For the other experimental conditions in which permeate flux decline is high (TMPs and crossflow velocities of 0.3 MPa and 1 m/s and 0.4 MPa and 2 m/s), the gel layer formation model (values of the R^2 for these experimental conditions are 0.942 and 0.829 according to Table 1, respectively) makes worse predictions than the complete (values of the R^2 for these experimental conditions are 0.977 and 0.975 according to Table 1, respectively) and the intermediate (values of the R^2 for these experimental conditions are 0.980 and 0.979 according to Table 1, respectively) blocking models.

For all the models considered in this work the precision in the fitted results is high when permeate flux slightly varies with time, this is for high crossflow velocities and low TMPs (Figs. 1–12). From the observation of Figs. 1, 4, 7 and 10 and Table 1 it can be concluded that the best fit to experimental data for a crossflow velocity of 1 m/s and a TMP of 0.4 MPa corresponds to the intermediate blocking model (the value of the R^2 for these experimental conditions is 0.997 according to Table 1) followed by the gel layer formation model (the value of the R^2 for these experimental conditions is 0.991 according to Table 1). This means that for the experimental conditions tested where fouling is more severe (1 m/s and 0.4 MPa) the predominant fouling mechanism is intermediate blocking according to the models. However, gel layer formation may also occur. This also implies that the cleaning procedure for the membrane fouled with PEG under these experimental conditions must be selected taking into account that the predominant type of fouling is intermediate blocking followed by gel layer formation. From the observation of Figs. 1–2, 4–5, 7–8 and 10–11 and Table 1 it can also be concluded that the best fit to experimental data for a crossflow velocity of 1 m/s and a TMP of 0.3 MPa and a crossflow velocity of 2 m/s and a TMP of 0.4 MPa corresponds to the intermediate blocking model (values of the R^2 for these experimental conditions are 0.980 and 0.979 according to Table 1, respectively) and to the complete block-

Table 1
Measures of fit, as per the R^2s, of Hermia's models.

TMP (MPa)	Crossflow velocity (m/s)	Measures of fit (R^2s)			
		Complete blocking	Intermediate blocking	Standard blocking	Gel layer
0.1	1	0.711	0.710	0.641	0.643
	2	0.724	0.725	0.703	0.651
	3	0.790	0.791	0.696	0.776
0.2	1	0.969	0.972	0.611	0.910
	2	0.925	0.923	0.765	0.777
	3	0.931	0.930	0.803	0.864
0.3	1	0.977	0.980	0.763	0.942
	2	0.985	0.984	0.920	0.983
	3	0.922	0.923	0.712	0.834
0.4	1	0.988	0.997	0.683	0.991
	2	0.975	0.979	0.615	0.829
	3	0.959	0.960	0.795	0.884

Table 2
Fitted parameters of Hermia's models for the Carbosep M2 membrane.

TMP (MPa)	Crossflow velocity (m/s)	K_c (m^{-1})	K_i (m^{-1})	$K_s \times 10^4$ ($s^{-0.5}\,m^{-0.5}$)	$K_{gl} \times 10^{-5}$ ($s\,m^{-2}$)
0.1	1	9.90	9.86	2.09	2.23
	2	4.13	4.09	1.34	1.24
	3	8.92	9.26	2.22	2.32
0.2	1	26.62	29.32	5.36	12.49
	2	8.95	9.24	3.38	1.15
	3	5.58	5.72	2.29	1.46
0.3	1	14.39	16.57	10.15	7.84
	2	4.08	4.09	4.50	1.95
	3	8.01	8.55	3.36	1.71
0.4	1	9.77	13.41	23.64	6.05
	2	12.85	15.17	7.09	2.57
	3	5.30	5.59	2.8	0.81

ing model (values of the R^2 for these experimental conditions are 0.977 and 0.975 according to Table 1, respectively).

Table 2 shows the values of the fitted parameters of Hermia's models for experimental data obtained with the Carbosep M2 membrane. According to the physical meaning and the definitions of the parameters of Hermia's models (Eqs. (4), (7), (9)), the values of these parameters should be higher when membrane fouling is more severe. This is consistent with the results showed in Table 2. Low crossflow velocities favour the accumulation of molecules near the membrane surface, i.e. fouling. According to this, the values of the fitted model parameters decrease with an increase in the crossflow velocity (less fouling). Nevertheless, the values of the fitted model parameters do not follow a clear tendency with TMP. This reveals that, as the adaptation of Hermia's models to crossflow ultrafiltration includes the effect of tangential flow on fouling of the membrane, the importance of effect of TMP on membrane fouling is not any more the main factor affecting permeate flux decline with time. The Hermia's models confer more importance to the effect of crossflow velocity on permeate flux. The values of the parameters of Hermia's models shown in Table 3 can also be estimated from the following empirical equations, Eqs. (10)–(13). These equations are valid for the experimental conditions where permeate flux decline during the ultrafiltration tests was significant (i.e. higher than 10%). These experimental conditions were a crossflow velocity of 1 m/s and TMPs of 0.3 and 0.4 MPa and a crossflow velocity (CFV) of 2 m/s and a TMP of 0.4 MPa.

$$K_c = 25.17 - 46.2(\mathrm{TMP}) + 3.08(\mathrm{CFV}) \quad (10)$$

$$K_i = 24.29 - 31.6(\mathrm{TMP}) + 1.76(\mathrm{CFV}) \quad (11)$$

$$K_s = -13.77 + 134.9(\mathrm{TMP}) - 16.55(\mathrm{CFV}) \quad (12)$$

$$K_{gl} = 16.69 - 17.9(\mathrm{TMP}) - 3.48(\mathrm{CFV}) \quad (13)$$

In Eqs. (10)–(13) TMP is expressed in MPa, CFV is expressed in m/s, K_c and K_i are expressed in m^{-1}, K_s is expressed in $10^{-4}\,s^{-0.5}\,m^{-0.5}$ and K_{gl} is expressed in $10^5\,s\,m^{-2}$.

Table 3 compares the experimentally measured initial permeate flux for the Carbosep M2 membrane and the initial permeate flux predicted by Hermia's models. The experimental error committed in the measures was inferior to 11%. Differences between measured and fitted initial permeate flux are inferior to the experimental error committed in the measures, except for the values marked with an asterisk. In this case, the differences were slightly superior to the experimental error committed in the measures except in the case of the standard blocking model for a TMP of 0.4 MPa and crossflow velocities of 1 m/s and 2 m/s. For these experimental conditions the difference between the measured and the fitted initial permeate flux was approximately 36% and 20%, respectively. Differences may be attributed to the difficulty in measuring permeate flux at the very early stages of ultrafiltration experiments. In the case of the standard blocking model these differences are due to the fact that fouling is caused by internal pore blocking. Therefore, fouling becomes independent of the crossflow velocity, which does not accurately describe experimental results (see Figs. 7–9).

Table 4 compares the experimentally measured steady-state permeate flux for the Carbosep M2 membrane and the steady-state permeate flux predicted by Hermia's models. The steady-state permeate flux predicted by the standard blocking model is omitted in Table 4. This model considers that no limiting value for the permeate flux is attained, i.e. steady-state permeate flux is zero [21]. In all cases, differences between the fitted and the experimentally mea-

Table 3
Comparison between the experimentally measured initial permeate flux for the Carbosep M2 membrane and the initial permeate flux predicted by Hermia's models.

TMP (MPa)	Crossflow velocity (m/s)	Initial permeate flux ($L\,h^{-1}\,m^{-2}$)				
		Complete blocking	Intermediate blocking	Standard blocking	Gel layer	Measured
0.1	1	35.90	35.90	35.50	36.08	34.62
	2	52.17	52.18	51.96	52.45	51.20
	3	64.42	64.46	63.04	64.29	63.04
0.2	1	48.28	48.49	43.16*	44.79	49.99
	2	72.77	72.80	70.43	72.04	70.56
	3	88.76	88.80	86.10	88.03	86.10
0.3	1	65.24	65.89	55.98*	61.54	65.46
	2	87.79	87.83	85.86	88.24	87.72
	3	114.88	115.10	108.43	113.23	116.95
0.4	1	153.41	159.34	103.93*	163.36	161.70
	2	115.95	117.32	95.95*	103.16*	119.33
	3	121.86	122.03	116.99	119.72	122.87

Table 4
Comparison between the experimentally measured steady-state permeate flux for the Carbosep M2 membrane and the steady-state permeate flux predicted by Hermia's models.

TMP (MPa)	Crossflow velocity (m/s)	Steady-state permeate flux ($L h^{-1} m^{-2}$)			
		Complete blocking	Intermediate blocking	Gel layer	Measured
0.1	1	33.56	33.53	27.85	34.07
	2	49.23	49.17	45.11	49.96
	3	59.17	59.15	56.49	59.13
0.2	1	38.38	38.32	37.62	38.25
	2	63.53	63.49	53.66	62.89
	3	78.78	78.66	76.39	79.09
0.3	1	43.36	43.03	40.99	42.96
	2	71.24	70.60	70.24	73.01
	3	96.37	96.24	93.65	95.62
0.4	1	51.07	48.12	41.48	45.71
	2	77.51	77.18	72.25	75.69
	3	104.09	103.95	98.58	104.55

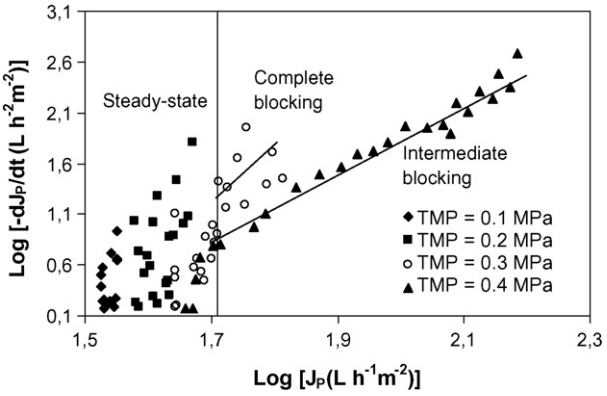

Fig. 13. Filtration curve $\log(-dJ_P/dt)$ versus $\log(J_P)$ for a crossflow velocity of 1 m/s and a solute concentration of 5 g/L for the Carbosep M2 membrane.

sured steady-state permeate fluxes are lower than the experimental error committed in the measures.

Hwang and Lin [17] used the filtration curves of dt/dV versus V during crossflow filtration to understand the mechanisms of pore blockage that corresponded to Hermia's models. A similar analysis for Hermia's models adapted to crossflow ultrafiltration is carried out is this work. In this case, the filtration curves of $\log(-dJ_P/dt)$ versus $\log(J_P)$ are divided in different regions that correspond to the different models. The filtration curves of $\log(-dJ_P/dt)$ versus $\log(J_P)$ are represented in Figs. 13–15. It can be observed that when permeate flux varies very slightly with time the filtration curves correspond to vertical straight lines. For the rest of experimental conditions, this is for a crossflow velocity of 1 m/s and a TMP of 0.3 MPa and 0.4 MPa and in the case of a crossflow velocity of 2 m/s and a TMP of 0.4 MPa, the filtration curves can be divided in two regions. In the first region the slope of the filtration curves can be used to estimate the parameter n in Eq. (2). In the second region, the filtration curves are vertical lines and their slope is infinite. This last region corresponds to steady-state conditions. The constant n was estimated for the experimental conditions where the permeate flux varied significantly with time. For the rest of experimental conditions tested steady-state was achieved practically from the beginning of ultrafiltration and the constant n could not be determined.

For the experimental data obtained in this work, estimation of the parameter n in Eq. (2) was more accurate for the experimental conditions where the permeate flux decline with time is the highest, these are a TMP of 0.4 MPa and a crossflow velocity of 1 m/s. The filtration curve for a TMP of 0.4 MPa and a crossflow velocity of 1 m/s can be divided in two regions (Fig. 13). At the beginning of ultrafiltration, the constant n in Eq. (2) can be regressed as 1.18. This reveals that intermediate blocking is dominant in this region. In the second region, the filtration rate remains constant and steady-state is achieved. This means that the flow of molecules towards the membrane is compensated by the tangential flow towards the membrane module exit. The filtration curve for a TMP of 0.3 MPa and a crossflow velocity of 1 m/s can also be divided in two regions (Fig. 13). In the first region, the Hermia's model becomes complete blocking since the constant n in Eq. (2) can be regressed to 2.8.

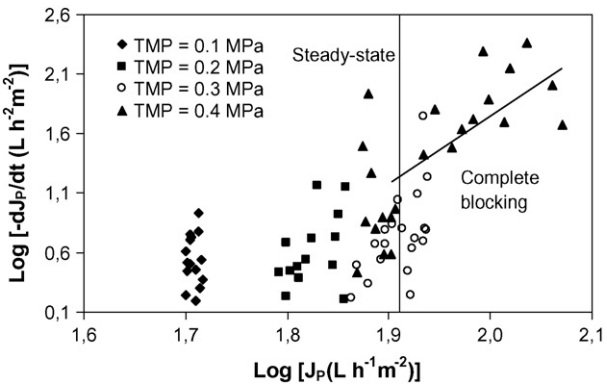

Fig. 14. Filtration curve $\log(-dJ_P/dt)$ versus $\log(J_P)$ for a crossflow velocity of 2 m/s and a solute concentration of 5 g/L for the Carbosep M2 membrane.

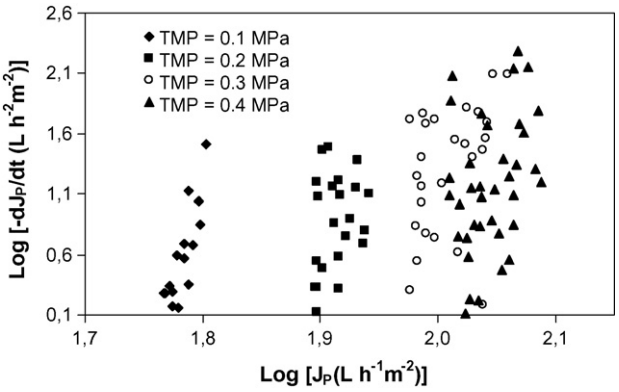

Fig. 15. Filtration curve $\log(-dJ_P/dt)$ versus $\log(J_P)$ for a crossflow velocity of 3 m/s and a solute concentration of 5 g/L for the Carbosep M2 membrane.

The second region corresponds to steady-state conditions. Finally, two regions are found in filtration curve for a TMP of 0.4 MPa and a crossflow velocity of 2 m/s (Fig. 14), which are the same as those described for a TMP of 0.3 MPa and a crossflow velocity of 1 m/s. The first region corresponds to complete blocking as n is regressed as 2.6. The values of n reported in this work are close to the theoretical values for the different Hermia's models. The deviations of the values of n from the theoretical values are attributed to the fact that the regions in the filtration curves are superimposed [18]. For the highest TMP and the lowest crossflow velocity tested, the flow of solute molecules towards the membrane surface and the accumulation of them over the membrane surface is the highest. Therefore, the probability of a solute molecule to lay over another solute molecule previously deposited on the membrane surface is the highest and intermediate blocking is more likely to occur than complete blocking for these experimental conditions. This is consistent with the results obtained in this work. The general expression for n as a function of t, TMP and CFV corresponds to Eq. (14). The time interval for the experiments not contemplated in Eq. (14) corresponds to steady state.

$$n = \left\{ \begin{array}{ll} 1.18 & \text{if TMP} = 0.4\,\text{MPa, CFV} = 1\,\text{m/s and } 0 \le t \le 1540\,\text{s} \\ 2.8 & \text{if TMP} = 0.3\,\text{MPa, CFV} = 1\,\text{m/s and } 0 \le t \le 3544\,\text{s} \\ 2.6 & \text{if TMP} = 0.4\,\text{MPa, CFV} = 2\,\text{m/s and } 0 \le t \le 7483\,\text{s} \end{array} \right\} \quad (14)$$

There were not found any significant differences in the determination of the fouling mechanisms by the two methods used: regression analysis of Eqs. (3), (5), (6), (8) and the filtration curves of $\log(-dJ_P/dt)$ versus $\log(J_P)$ (Eq. (2)). The regression analysis as well as the filtration curve analysis revealed that the phenomenon controlling fouling was intermediate blocking for a TMP of 0.4 MPa and a crossflow velocity of 1 m/s. For a TMP of 0.3 MPa and a crossflow velocity of 1 m/s and for a TMP of 0.4 MPa and a crossflow velocity of 2 m/s, complete blocking controlled the fouling process when both the regression analysis and the filtration curve analysis were used. However, the regression analysis was also accurate when intermediate blocking was considered.

5. Conclusions

According to Figs. 1–12, all the models considered in this work fit very accurately to the experimental data when permeate flux slightly decreases with time. Therefore, the most appropriate model for certain experimental data on flux decline can only be selected when permeate flux decreases noticeably with time. The best fit to experimental data for the following experimental conditions, crossflow velocities and TMPs, correspond to the following models: 1 m/s and 0.4 MPa (the intermediate blocking model followed by the gel layer formation model), 1 m/s and 0.3 MPa (the intermediate and the complete blocking models) and 2 m/s and 0.4 MPa (the intermediate and the complete blocking models). From the observation of Figs. 1–12 and the values of the R^2 in Table 1, it can be concluded that the standard blocking model fits worse to the experimental data than the other models considered in this work. It can also be concluded that the intermediate blocking model fits accurately to experimental data for all the experimental conditions tested.

The values of the fitted parameters of Hermia's models decrease with an increase in the crossflow velocity (less fouling). This is consistent with the physical meaning of the parameters. Nevertheless, the values of the fitted model parameters do not follow a clear tendency with TMP. For most of the experimental conditions tested, differences between measured and fitted initial permeate flux and differences between measured and fitted steady-state permeate flux are inferior to the experimental error committed in the measures.

The constant n could only be estimated for the filtration curves were the permeate flux varied significantly with time. Estimation of the constant n from the curves of $\log(-dJ_P/dt)$ versus $\log(J_P)$ was performed by dividing these curves in different regions. The filtration curve for a TMP of 0.4 MPa and a crossflow velocity of 1 m/s revealed that intermediate blocking was dominant. In the filtration curves for a TMP of 0.3 MPa and a crossflow velocity of 1 m/s and in the case of a TMP of 0.4 MPa and a crossflow velocity of 2 m/s, the corresponding Hermia's model was complete blocking.

There were found no significant differences in the determination of the fouling mechanism by the two methods used: regression analysis of Eqs. (3), (5), (6), (8) and the filtration curves of $\log(-dJ_P/dt)$ versus $\log(J_P)$ (Eq. (2)).

Acknowledgements

The authors of this work wish to gratefully acknowledge research assistance by Juan Manuel García Lara and José Luís Guiñón Segura and the financial support of the Spanish Ministry of Science and Technology (MCYT) through the project no. CTQ2005-03398.

References

[1] H.K. Shon, S. Vigneswaran, I.S. Kim, J. Cho, H.H. Ngo, Effect of pretreatment on the fouling of membranes: application in biologically treated sewage effluent, J. Membr. Sci. 234 (2004) 111–120.
[2] M. Cheryan, J.R. Alvarez, Food and beverage industry applications, in: R.D. Noble, S.A. Stern (Eds.), Membrane Separation Technology—Principles and Applications, Elsevier, Amsterdam, The Netherlands, 1995, p. 341.
[3] R. Chan, V. Chen, Characterization of protein fouling on membranes: opportunities and challenges, J. Membr. Sci. 242 (2004) 169–188.
[4] F. Lipnizki, Opportunities and challenges of using ultrafiltration for the concentration of diluted coating materials, Desalination 224 (2008) 98–104.
[5] J.M. Gozálvez-Zafrilla, D. Sanz-Escribano, J. Lora-García, M.C. León Hidalgo, Nanofiltration of secondary effluent for wastewater reuse in the textile industry, Desalination 222 (2008) 272–279.
[6] A.L. Ahmad, S. Ismail, S. Bhatia, Water recycling from palm oil mill effluent (POME) using membrane technology, Desalination 157 (2003) 87–95.
[7] K. Trivunac, S. Stevanovic, Removal of heavy metal ions from water by complexation-assisted ultrafiltration, Chemosphere 64 (2006) 486–491.
[8] W. Scholz, M. Lucas, Techno-economic evaluation of membrane filtration for the recovery and re-use of tanning chemicals, Water Res. 37 (2003) 1859–1867.
[9] N. Laitinen, A. Luonsi, E. Levänen, M. Nyström, Effect of backflushing conditions on ultrafiltration of board industry wastewaters with ceramic membranes, Sep. Purif. Technol. 25 (2001) 323–331.
[10] R.W. Field, D. Wu, J.A. Howell, B.B. Gupta, Critical flux concept for microfiltration fouling, J. Membr. Sci. 100 (1995) 259–272.
[11] S.T.D. de Barros, C.M.G. Andrade, E.S. Mendes, L. Peres, Study of fouling mechanism in pineapple juice clarification by ultrafiltration, J. Membr. Sci. 215 (2003) 213–224.
[12] P.K. Bhattacharya, S. Agarwal, S. De, U.V.S. Rama Gopal, Ultrafiltration of sugar cane juice for recovery of sugar: analysis of flux and retention, Sep. Purif. Technol. 21 (2001) 247–259.
[13] C. Bhattacharjee, S. Datta, Analysis of polarized layer resistance during ultrafiltration of PEG-6000: an approach based on filtration theory, Sep. Purif. Technol. 33 (2003) 115–126.
[14] J. Hermia, Constant pressure blocking filtration laws—application to power-law non-newtonian fluids, Trans. Inst. Chem. Eng. 60 (1982) 183–187.
[15] S. Ganguly, P.K. Bhattacharya, Development of concentration profile and prediction of flux for ultrafiltration in radial cross-flow cell, J. Membr. Sci. 97 (1994) 185–198.
[16] S. Ghose, C. Battacharjee, S. Datta, Simulation of unstirred batch ultrafiltration process based on a reversible pore-plugging mode, J. Membr. Sci. 169 (2000) 29–38.
[17] K.-J. Hwang, T.-T. Lin, Effect of morphology of polymeric membrane on the performance of cross-flow microfiltration, J. Membr. Sci. 199 (2002) 41–52.
[18] W.R. Bowen, J.I. Calvo, A. Hernández, Steps of membrane blocking in flux decline during protein microfiltration, J. Membr. Sci. 101 (1995) 153–165.
[19] A.B. Koltuniewicz, R.W. Field, Process factors during removal of oil-in-water emulsions with cross-flow microfiltration, Desalination 105 (1996) 79–89.
[20] T. Mohammadi, M. Kazemimoghadam, M. Saadabadi, Modeling of membrane fouling and flux decline in reverse osmosis during separation of oil in water emulsions, Desalination 157 (2003) 369–375.
[21] S. Todisco, L. Peña, E. Drioli, P. Tallarico, Analysis of the fouling mechanism in microfiltration of orange juice, J. Food Process. Preserv. 20 (1996) 453–466.

[22] S. Sommer, T. Melin, Influence of operation parameters on the separation of mixtures by pervaporation and vapor permeation with inorganic membranes. Part 2: Purely organic systems, Chem. Eng. Sci. 60 (2005) 4525–4533.
[23] T.K. Sen, M.V. Sarzali, Removal of cadmium metal ion (Cd^{2+}) from its aqueous solution by aluminium oxide (Al_2O_3): a kinetic and equilibrium study, Chem. Eng. J. 142 (2008) 256–262.
[24] A. Bhatnagar, A.K. Minocha, D. Pudasainee, H.-K. Chung, S.-H. Kim, H.-S. Kim, G. Lee, B. Min, B.-H. Jeon, Vanadium removal from water by waste metal sludge and cement immobilization, Chem. Eng. J. 144 (2008) 197–204.
[25] H. Choi, K. Zhang, D.D. Dionysiou, D.B. Oerther, G.A. Sorial, Effect of permeate flux and tangential flow on membrane fouling for wastewater treatment, Sep. Purif. Technol. 45 (2005) 68–78.
[26] P. Blanpain-Avet, L. Fillaudeau, M. Lalande, Investigation of mechanisms governing membrane fouling and protein rejection in the sterile microfiltration of beer with an organic membrane, Food Bioproducts Process. 77 (1999) 75–89.
[27] M.C. Vincent-Vela, S. Álvarez-Blanco, J. Lora-García, J.M. Gozálvez-Zafrilla, E. Bergantiños-Rodríguez, Modelling of flux decline in crossflow ultrafiltration of macromolecules: comparison between predicted and experimental results, Desalination 204 (2007) 328–334.
[28] M.C. Vincent-Vela, S. Álvarez-Blanco, J. Lora-García, J.M. Gozálvez-Zafrilla, E. Bergantiños-Rodríguez, Utilization of a shear induced diffusion model to predict permeate flux in the crossflow ultrafiltration of macromolecules, Desalination 206 (2007) 61–68.
[29] Z. Gu, Across-Sample Incomparability of R^2s and Additional Evidence on Value Relevance Changes Over Time, Carnegie Mellon Univeristy, 2004.